Imaging and Quantitative Assessment of Long Bone Vascularization in the Adult Rat Using Microcomputed Tomography

Fei Jia, Françoise Peyrin, Luc Malaval, Laurence Vico, Marie-Hélène Lafage-Proust

Imaging and Quantitative Assessment of Long Bone Vascularization in the Adult Rat using Microcomputed Tomography

FEI JIA,[1,2] PEYRIN FRANÇOISE,[1,3] LUC MALAVAL,[1,2] VICO LAURENCE,[1,2] AND LAFAGE-PROUST MARIE-HÉLÈNE[1,2*]
[1]Université de Lyon, Lyon, France
[2]INSERM U890, IFR 62, Saint-Etienne, France
[3]ESRF, INSERM-630, CRS-5515, Lyon, France

ABSTRACT

The objective of this study was to develop and validate a technique for both 3D imaging and quantification of the vascular network of bone tissue in the rat. Five month-old male Wistar rats were divided into tail-suspension (21 days) and control groups. Sixty percent barium sulfate solution was infused into the vena cava. The tibiae were evaluated in 2D and 3D before and after decalcification, using conventional microcomputerized tomography (μCT) at 10 and 5 μm resolution and synchrotron radiation (SR) μCT. The perfusion technique and tomography exhibited excellent bone vasculature imaging. Significant positive correlations were observed between 2D histomorphometric and 3D μCT vascular parameters ($P < 0.05$). 3DμCT discriminated significant changes of vessel structures in unloading condition: vessel number decreased by 25%, ($P < 0.005$), vessel separation increased by 27%, $P < 0.01$. SRμCT could image sinusoid clusters in bone. μCT is an accurate and reproducible technique for 3D quantitative evaluation of long bone vascularisation in the rat. Anat Rec, 293:215–224, 2010. © 2009 Wiley-Liss, Inc.

Key words: quantitative microcomputed tomography analysis; vascularization; bone marrow; rat; tibia

INTRODUCTION

While providing mechanical support for locomotion, bone is the major calcium storage and management pool of the organism and it is also the site of hematopoiesis. Interestingly, bone vascularization represents the anatomical and functional link between these three different functions. Bone vessels, when organized in clusters of sinusoids, play a major role in the hematopoietic niche (Schatteman and Awad, 2004). The role of bone vascularization during growth or fracture repair and malignant diseases such as metastasis (Yin et al., 2005) or myeloma (Harousseau et al., 2004) has been established. Its involvement in bone remodeling in adults and metabolic bone diseases such as osteoporosis is not well understood. For instance, in the rat, an hindlimb unloading experiment which simulates microgravity, the blood perfusion in femur, tibia and bone marrow were significantly decreased. This blood supply change corresponded to the unloading-induced bone loss (Colleran et al., 2000). This suggested that bone vascularization might be implicated in the unloading-induced bone loss.

Imaging and quantification of the bone vessel network (Kan et al., 2005) are a prerequisite for the better understanding of its function. Imaging of the three-dimensional architecture of the microvascular bed has been reported for many tissues such as heart (Toyota et al., 2002), kidney (Fortepiani et al., 2003) or brain

*Correspondence to: Lafage-Proust Marie-Hélène, Equipe INSERM U890, Université Jean Monnet, Faculté de Médecine; 15, rue Ambroise Paré, 42023, St-Etienne, Cedex 2, France. Fax: 33 (0) 477127577. E-mail: lafagemh@univ-st-etienne.fr

Received 4 February 2009; Accepted 11 August 2009
DOI 10.1002/ar.21054
Published online 2 December 2009 in Wiley InterScience (www.interscience.wiley.com).

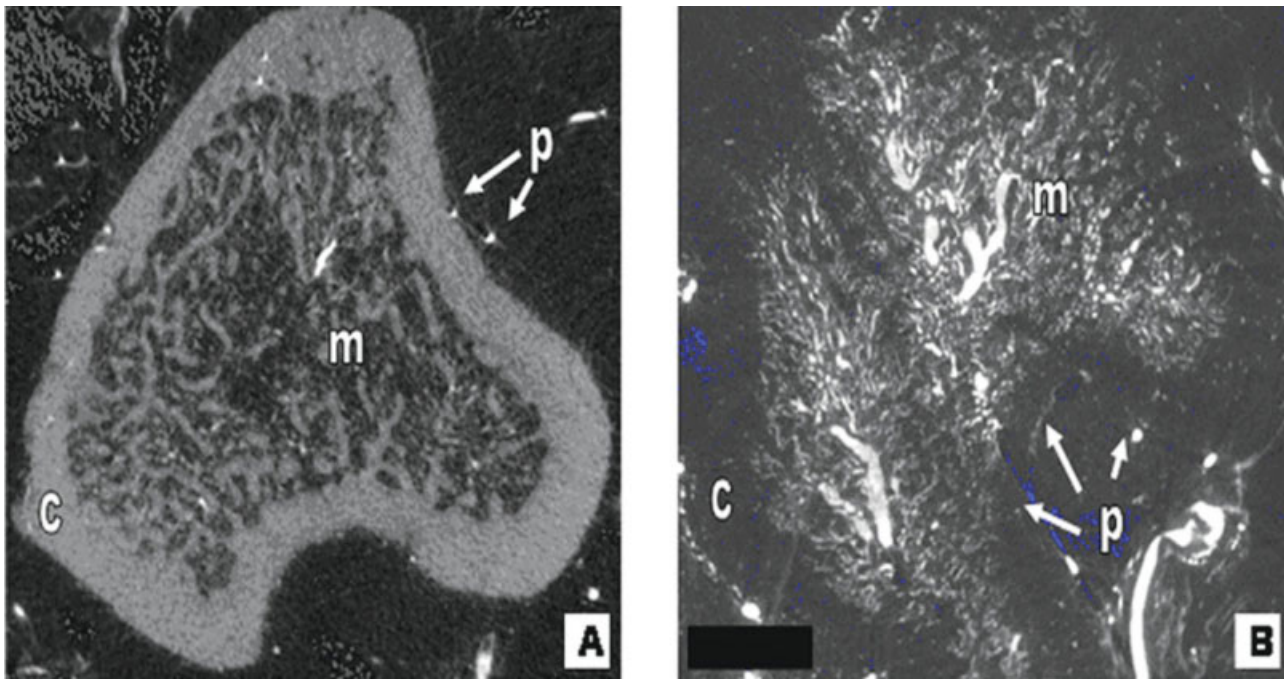

Fig. 1. Images of tibia metaphysis transverse sections obtained with VivaCT40 at 10 μm resolution. (**A**) Nondecalcified bone showing little contrast between bone and vessel signals. (**B**) Decalcified bone image, showing homogenous opacification of the bone vessel network. c: cortex. m: marrow. p: periosteal vessels.

(Plouraboue et al., 2004) in rodents. In contrast, very little data on bone vessels in terms of 3D anatomy are available, whereas quantitative information of their spatial organization would bring greater insights on the pathophysiology of bone diseases (Plouraboue et al., 2004) or on the mechanisms of action of treatments. Indeed, so far, the bone vasculature has been mainly investigated in bone sections analyzed by optical microscopy either after vessel opacification with a contrast agent (India ink), or using histoenzymology or immunohistochemistry techniques with antibodies directed against endothelial markers (Lundberg et al., 2000) or extracellular matrix proteins (Mark et al., 2004). Although these methods can be very accurate, they survey a very limited tissue area and can miss some vascular structures (Barou et al., 2002). Other studies using plastic vascular casts followed by scanning electron microscopy mainly reported analyses of the growth plate blood supply. X-ray computed microtomography (μCT) exhibits several advantages: it provides stacks of high resolution images allowing 3D reconstruction and it does not damage the samples. An in vivo neovascularization has been recently measured using μCT on engineered bone constructs (Bolland et al., 2008). Two types of 3D μCT techniques are currently used for imaging and quantification purposes: conventional X-ray μCT and Synchrotron Radiation μCT (SRμCT) (Elliott et al., 1994; Momose et al., 1996; Sasov and Van Dyck, 1998), which differ in terms of resolution, X-ray beam quality and availability.

The purpose of the present study was to develop a method based on vascular opacification to improve image quality, and evaluate bone vessel imaging using 3D μCT. Furthermore, we quantified the microvascular organization pattern of long bones in the rat. We induced bone vessel network changes in an unloading model of osteopenia to test our method and validate it by comparing the results to those obtained from bone histomorphometry.

MATERIALS AND METHODS

Animals

Twenty five month-old male Wister rats (483 ± 38 g) (Charles River Laboratories, l'Arbresle, France) were fed with a standard laboratory diet (rat chow) and water ad libitum. Rats were kept in standard conditions: temperature: 21.0°C ± 2.0°C, humidity: 55.0% ± 5.0% with a 12:12 hr light/dark cycle (07:00–19:00). The procedure for the care of the animals was in accordance with the European Community standards on the care and use of laboratory animals (Ministère de l'Agriculture, France, Authorization 04827).

To induce changes in bone vascularisation, we used the tail-suspension unloading model which leads to hindlimb osteopenia. Briefly, rats were either tail-suspended by using orthopedic tape (unload, $n = 8$), or kept in regular cages as controls (CTRL, $n = 12$) for 21 days. Tail suspension allowed the animals to move freely in specifically designed cages (Morey et al., 1979).

Vascular Bed Infusion Procedure and Sample Preparation

Before sacrifice, rats were injected subcutaneously with 300 IU/Kg heparin. After 1 hr, they were

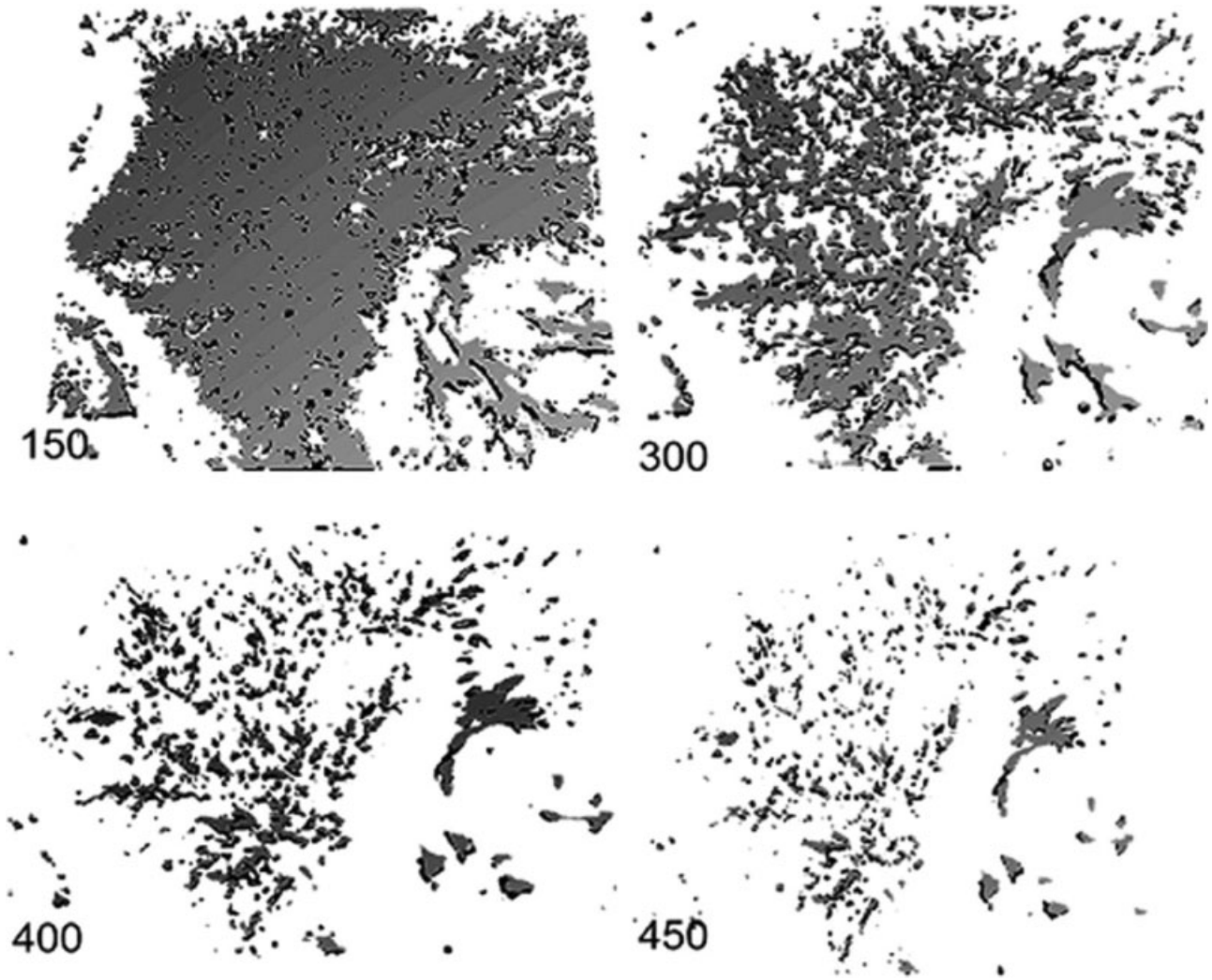

Fig. 2. Threshold variation influence on vascular quantification. Fifty slice-thick sections obtained from VivaCT40 scanning on one decalcified tibia metaphysis with increasing the threshold values (from 150 to 450).

euthanized by an intraperitoneal injection of sodium pentobarbital (2.0 mg/Kg). The thoracic cage was incised at the sternum level and the upper part of the rib cage was removed. The left ventricle was then punctured with a 22 G catheter (Insyte W, Becton Dickinson, France) and the right auricle sectioned to permit the elution of the infused solutions. The vascular network was first rinsed with 50 mL of a warm (37.0°C) PBS saline solution containing 10% glycerin, 15 UI/mL heparin, using a peristaltic pump (MasterFlex, L/S, model: 7553–7579, Cole-Parmer instrument). The posterior vena cava was then isolated and catheterized, and the contrast agent [60% barium, (Micropaque® suspension, Guerbet, Paris, France, Ref: 400301658), 0.1% light green diluted in PBS (potassium chloride 2.68 mM, potassium phosphate monobasic 1.47 mM, sodium chloride 136.89 mM, sodium phosphate dibasic 8.10 mM)] was infused. All infusion procedures were performed with the following hydrodynamic parameters: infusion velocity = 25 mL/min, pulse frequency = 1.67 Hz; the pressure was controlled with a manometer (02.4 × DN 100–150, TEMPCO, Belgium) and set at 150–200 mmHg. Adequacy of infusion was assessed when the ears, the eyes, and the tail were fully stained green. About 100 mL of the contrast solution was allowed to flow through the vascular bed. After infusion, the left tibiae were removed and processed for histomorphometry and the right tibiae were removed and imaged using high resolution microcomputed tomography (μCT). The tibiae were then decalcified for 21 days in 10% EDTA and imaged again with μCT.

Histomorphometric Analysis

Left tibiae were fixed in 10% formaldehyde solution, dehydrated in absolute acetone, and embedded in methylmethacrylate at low temperature as previously developed in our laboratory (Chappard et al., 1987). Eight micrometer frontal sections were cut using a Polycut microtome (Reichert, Paris, France) and prepared for

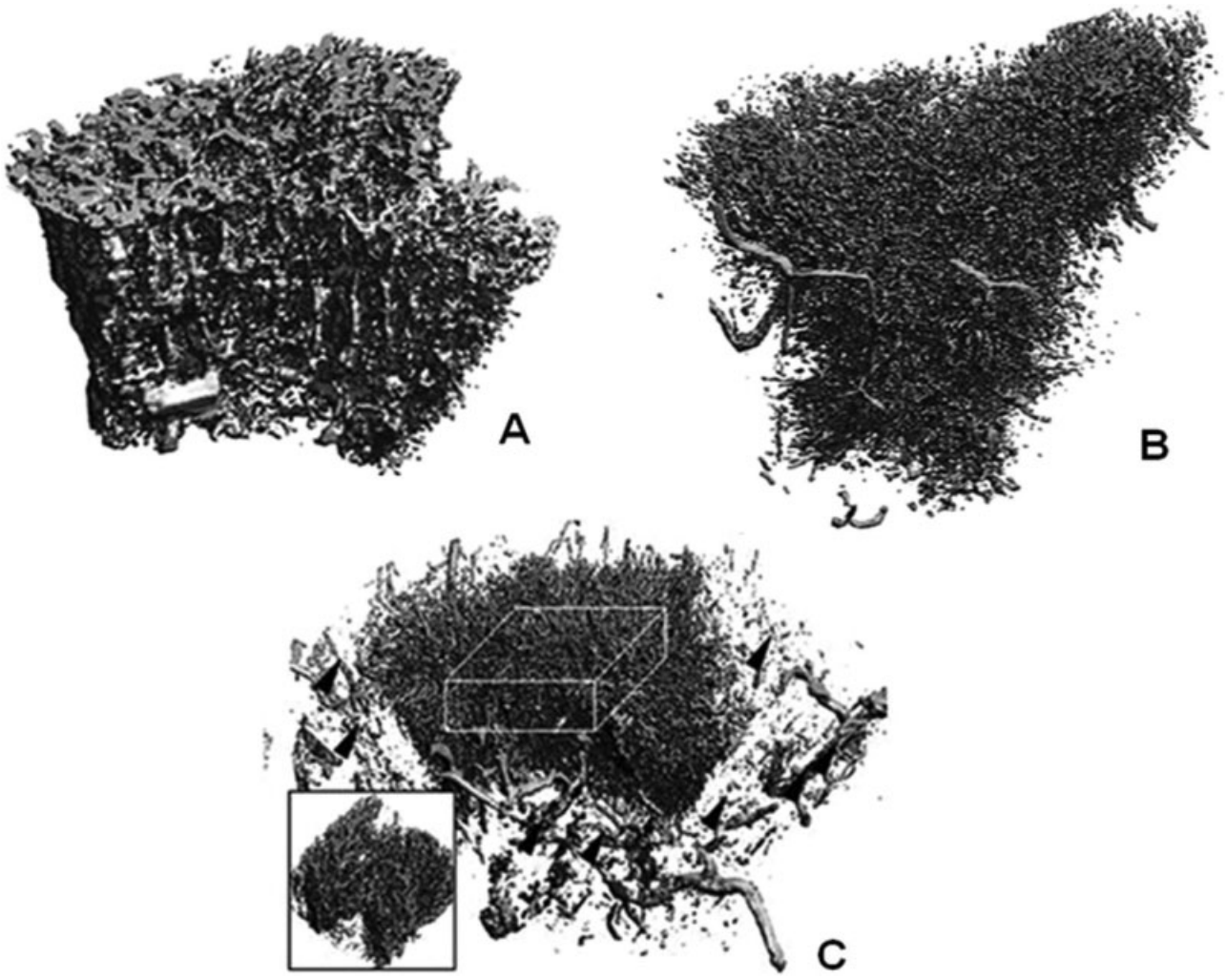

Fig. 3. Three dimensional vessel imaging of tibia metaphysis using conventional microtomography (**A**, **B**: 10 μm resolution, VivaCT40; **C**: 5 μm resolution, μCT 40) before (A) and after bone decalcification in EDTA (B, C). A: Representative image showing the lack of discrimination between bone and vessel signals. B: Visualization of the bone vessel network. C: Inserting the ROI (1.8 × 1. 9 × 1 mm, empty cube) drawn from the image for vessel quantification. Black arrow heads: subperiosteal vessels.

quantitative bone histomorphometric measurements, as described (Parfitt et al., 1987).

Quantification of vascular parameters. Four unstained sections from each barium sulfate-infused tibia were analyzed at a 100× magnification. Twelve fields per section, covering the whole secondary spongiosa were quantified. Binary images were made and analyzed using the IMAGEJ PC-based software (National Institute of Health, NIH Version v1.32j, http://rsb.info.nih.gov/ij). The analyses included the mean number of vessels/mm^2 of tissue volume (VN/TV, Nb/mm^2) and the vascular volume/tissue volume (VV/TV, %). The intraindividual coefficients of variation for vessel number and volume measurements were 2.5 and 2.7%, respectively.

Microcomputed X-ray Tomography (μCT)

Bone samples, undecalcified and decalcified, were imaged by high resolution tomography scanning (μCT) using a VivaCT40 (Scanco Medical AG, Basserdorf, Switzerland). The spatial resolution was fixed at 10 μm. The filtered (0.3 mmAl) 45 keV X-ray spectrum was set at 25 keV. For each sample, a total of 347 microtomographic slices with a slice increment of 10 μm was acquired, covering 4 mm of the metaphysis length. The measurements were stored in 3D image arrays (1024 × 1024 × 286 voxels; 32,767 gray values). Within this data set, a selected region of interest (ROI, 1.8 × 1.9 × 1 mm) of 100 microtomographic slices was defined in the centre of the secondary spongiosa (IISP), as shown in Fig. 3C. Binary images were prepared using the same parameters (sigma = 1, filter support = 2, and threshold values = 10.2% of maximal possible gray value, i.e. 300 for this evaluation). The following three-dimensional vascular parameters were measured: vascular volume/tissue volume (VV/TV, %), mean number of vessels (V.N, /mm), mean vessel thickness (V.Th, μm) and mean vessel separation (V.Sp, μm), using the software available for bone

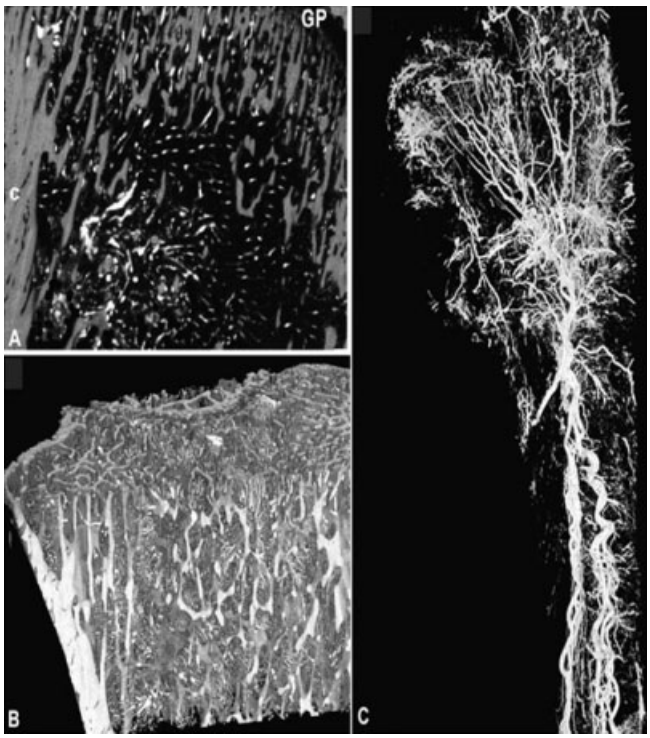

Fig. 4. Synchrotron radiation microtomography images of undecalcified (**A**, **B**) and decalcified tibiae (**C**) on 5 μm resolution. Raw slice (A) and 3D display (B) of a nondecalcified tibia metaphysis. Note that the reconstructed attenuation values in vessels (white) and in bone (gray) may clearly be distinguished. C: Decalcified tibia vascularization obtained merging seven regions of interest. In Figure 4A, C: cortex. GP: growth plate.

microarchitecture measurements (Software Revision 3.2; Scanco Medical). Briefly, the vascular volume fraction was measured directly by plotting gray voxels against black voxels (nonvessel objects) in the volume of interest (VOI) (VOX VV/TV). Vascular volume (VV) and vascular surface (VS) were calculated using a tetrahedron meshing technique generated by the "marching cubes method" (Lorensen and Cline, 1987) and total volume (TV) was calculated as the volume of interest (VOI). V.Th was defined as twice VV/VS, V.Sp as 2(TV-VV)/VS, and V.N as 0.5VS/TV (Parfitt et al., 1983). V.N was determined by analogy with the V.Sp calculation. However, V.N was the inverse of V.Sp. The coefficients of variation (CV) were 10.2% for VV/TV, 6.0% for V.N, 9.4% for V.Th, 6.6% for V.Sp.

A subset of decalcified tibiae were also imaged at 5 μm resolution on the μCT40 apparatus (Scanco Medical AG, Basserdorf, Switzerland), using a procedure similar to VivaCT40 imaging.

Synchrotron Radiation Microtomography

Decalcified and nondecalcified bone opacified with barium sulfate, were also imaged using SRμCT at the ESRF (European Synchrotron Radiation Facility, Grenoble, France). The experiment was performed on a beam line (ID-19), which gives a spatial resolution between 10 μm and 0.3 μm (Salome et al., 1999). A $(2048)^2$ CCD based detector and a pixel size of 4.9 mm was used. The scanned area was about 10 mm and covered the whole tibiae. A ROI of 1700 × 800 pixels was adjusted on the detector to cover a height of ~4 mm in the metaphysis region. The slits limiting the beam were adjusted accordingly so as to limit scattered radiation. To maximize the flux and reduce acquisition time, we used synchrotron radiation emitted from an ondulator (gap ~17 mm). The energy was set to 23.3 keV. The exposition time in each radiograph was 0.7 sec yielding a total acquisition time of about 30 min per sample. A VOI of 1300 × 1300 × 800 voxels was then reconstructed using a customized 3D slice by slice version of the filtered backprojection algorithm implemented at ESRF. The voxel size in the 3D image is isotropic and equal to 4.9 μm.

Statistical Analysis

Statistical analysis was performed with STATISTICA software (StatSoft, Tulsa, OK). For vascular parameters, the differences between groups were analyzed with the nonparametric Mann-Whitney U test. Histomorphometry and μCT measurements were compared by Pearson correlation analysis. A $P < 0.05$ value was considered to be significant.

RESULTS

Bone Vessel Micro-Tomography

Conventional μCT. Transverse μCT images of bones, obtained with the VivaCT40 apparatus (10 μm resolution), showed little contrast between bone and vessel signal (Fig. 1A). Indeed, while the medium size vessels seen in the subperiosteal region were clearly visible, the smaller ones, within the bone marrow, were barely distinguishable from the bone trabeculae. In contrast, in decalcified bones, the vessel network was distinctly imaged. Opacification was homogenous and the vascularization was so dense that the bone trabecular network appeared in black, as a negative image (Fig. 1B). Although some small vessels in the cortices could be observed, the cortical network was not fully visualized.

Figure 2 illustrates the influence of threshold values on the morphology of the vascular tree. As expected, with the highest thresholds we obtained the most accurate images of the larger vessels, while the smallest ones were omitted. In contrast, with lower thresholds, the smallest vessels could remain part of the image, while the biggest ones appeared artifactually large because of the partially filled voxels surrounding them. Using increasing thresholds led to decreasing vascular volume/tissue volume measured on binary images (89.5%, 21.7%, 12.4%, and 5.2% for threshold values of 150, 300, 400, and 450, respectively). A threshold value at 300 was found to be the best optimal compromise for vessel imaging and quantification. The chosen threshold was shown to keep a homogeneous measuring range of data among the different samples.

Figure 3 illustrates the 3D images obtained from the undecalcified (A) or decalcified samples (B, C). The volume rendering images obtained from nondecalcified bones led to a dense complex which was the result of two intricate networks of bone and vessels (Fig. 3A). In decalcified bones, the vessel network was clearly identifiable with, as expected, a better definition of the

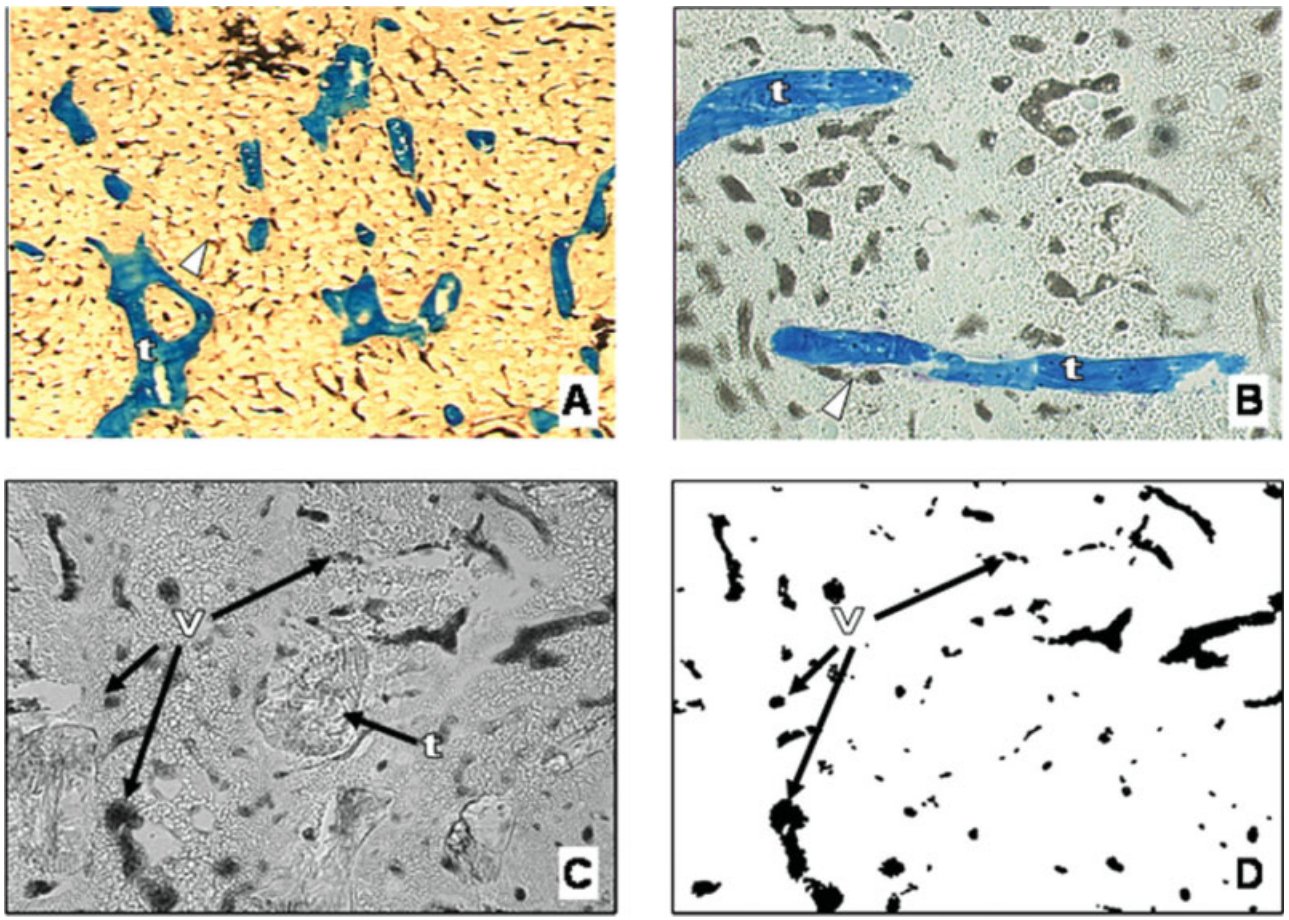

Fig. 5. Histological frontal 12 μm -thick sections of undecalcified tibia metaphysis at 100× (**A**) and 250× (**B**) original magnifications showing the vessel network homogenously opacified by barium sulfate infusion. Arrow head: vessel. Vascular quantification was performed on bone histological unstained sections. (**C**) Light microscopy image (100×) vessels (v). (**D**) After image acquisition and treatment by the IMAGEJ 1.32J software, trabecula and background were removed and the remaining capillaries were quantified. t: trabecula.

anatomical structures at 5 μm (3C) than at lower resolution (3B).

Synchrotron radiation imaging. Figure 4A,B respectively illustrate a raw slice and a 3D display of a nondecalcified infused tibia metaphysis, imaged with SRμCT. Unlike the images obtained with conventional μCT, the reconstructed attenuation values in vessels (white) and in bone (gray) can be clearly distinguished. The linear attenuation coefficient was ~4 cm^{-1} in large vessels, and between 3 and 5 cm^{-1} in bone. However, the linear attenuation histograms showed an overlapping of the bone and vessels peaks (not shown). One decalcified sample was also imaged in similar conditions so as to visualize the quasi-entire vascular region in the tibia (Fig. 4C).

Bone Vessel Histology

As shown in Fig. 5A, the technique used for barium sulfate infusion allowed adequate opacification of the vessel network which appeared dense and homogenous. Of note, the infusion is efficient enough to penetrate the layout of smaller vessels surrounding bone trabeculae (Fig. 5B).

Quantification of Vessel Parameters

We measured bone vessel number and volume in tibia metaphysis of control and tail-suspended rats using both quantitative histomorphometry and μCT. Figure 5C,D shows the results of image treatment histology sections, which included a step of auto-thresholding followed by a smoothing step and background removal by exclusion of objects smaller than 10 pixels. We found that the 3D μCT parameters, measured at 10 μm resolution, correlated significantly with those measured on 2D histological sections: ($r = 0.76$, $P < 0.0005$, Fig. 6A and $r = 0.74$, $P < 0.001$, Fig. 6B; $r = 0.56$, $P < 0.05$, Fig. 6C; for vessel volume, number and mean area, respectively). Unloading induced a significant 25% ($P < 0.005$) decrease in vessel number, associated with a significant increase 27% ($P < 0.01$) in vessel separation, with a nonsignificant decrease in vessel volume and no change in

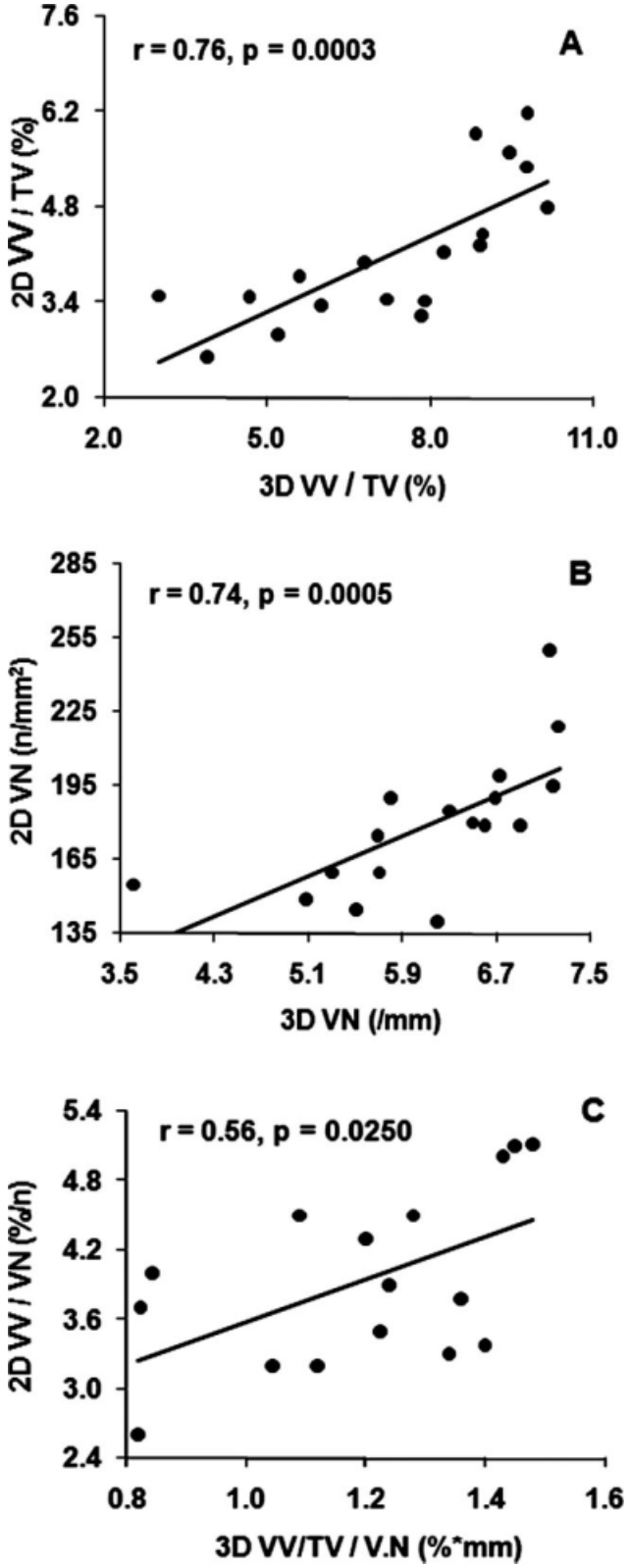

Fig. 6. Significant positive correlation between 2D histological and 3D μCT (VivaCT40) quantitative measurements of bone vascularization. (**A**) Vascular volume/tissue volume (VV/TV), (%); (**B**) Vascular number (VN)/tissue volume; (**C**) Vascular volume/vascular number (VV/VN).

TABLE 1. μCT quantification of vessel number and vessel separation in unloading[a]

Group	VV/TV (%)	V.Th (μm)	V.Sp (μm)	V.N
CTRL	7.4 ± 2.0	30.0 ± 4.3	161.9 ± 19.9	6.4 ± 0.8
SUS	6.3 ± 2.2	28.3 ± 3.7	204.7 ± 31.6**	5.1 ± 0.8***

[a]Value are presented as means ± SEM (standard error of the mean).
$P < 0.01$.
***$P < 0.005$.

vessel mean thickness (Table 1, Fig. 7A,B). These results were coherent with the histomorphometric results (data not shown). Interestingly, when we measured vascular parameters on a subset of bone from the control group using the 5 μm resolution μCT 40, we found values of similar order, albeit higher than at 10 μm (e.g., VV/TV = 10.4 ± 3.6, N = 4, vs. 7.4 ± 2.0, N = 10).

Imaging of Bone Marrow Sinusoid Clusters

In the bone marrow, a subgroup of capillaries, also called sinusoids, exhibit, in particular regions, a specific spatial organization described as "clusters" or "clumps" of highly anastomosed vessels which are supplied by their own arteriole and drained by their own veins (Brookes, 1960). We were able to visualize these structures on histological sections, in various areas of long bones such as epiphyses, bone marrow and in the vicinity of bone cortices, as illustrated in Fig. 8A–D. Since sinusoid clusters are rather bulky structures (>300 μm), they could be identified on 2D slices of nondecalcified bone using VivaCT40 microtomography at 10 μm resolution (Fig. 8E,F). The 3D visualization of the ball-shaped sinusoid clusters within the marrow of long bones was shown on the image reconstruction after eliminating the smaller vessels with a size threshold procedure (Fig. 8G).

DISCUSSION

To our knowledge, this is the first quantitative study on long bone vascularization using 3D microtomography. In the present study, we show a new and reproducible procedure for visualizing and quantifying the bone vasculature in rat tibiae. An important assumption for quantitative assessment of bone vessels was that the barium sulfate mixture completely filled the vascular bed and did not leak out of the vessels after the infusion. Therefore we set up a new infusion procedure to make a better perfusion of contrast solution in bone marrow. Furthermore, sinusoids and the terminal arteries are difficult to infuse, because of their fragile structure. Thus, the infused solutions included 10% glycerin to increase viscosity and ensure laminar flow. Duvall et al. 2004 used lead chromate suspended in a silicon-based polymer for imaging peripheral vascularization in mice hindlimbs, and found that the image quality was better than that obtained with barium sulfate. This contrast agent has been also used for evaluating bone grafts (de Magalhaes et al., 1998), flat bone vascularization

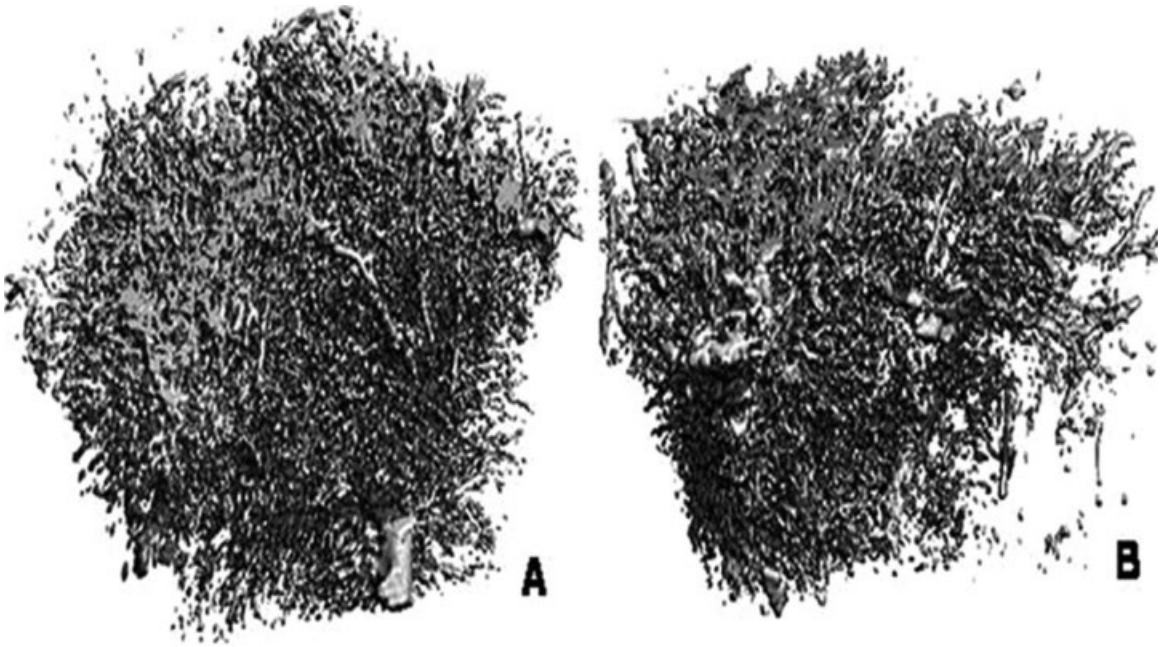

Fig. 7. Representative image of decalcified tibia metaphysis obtained from control rats (**A**) and tail suspended rats for 21 days (**B**) illustrating the decrease in vessel volume induced by unloading.

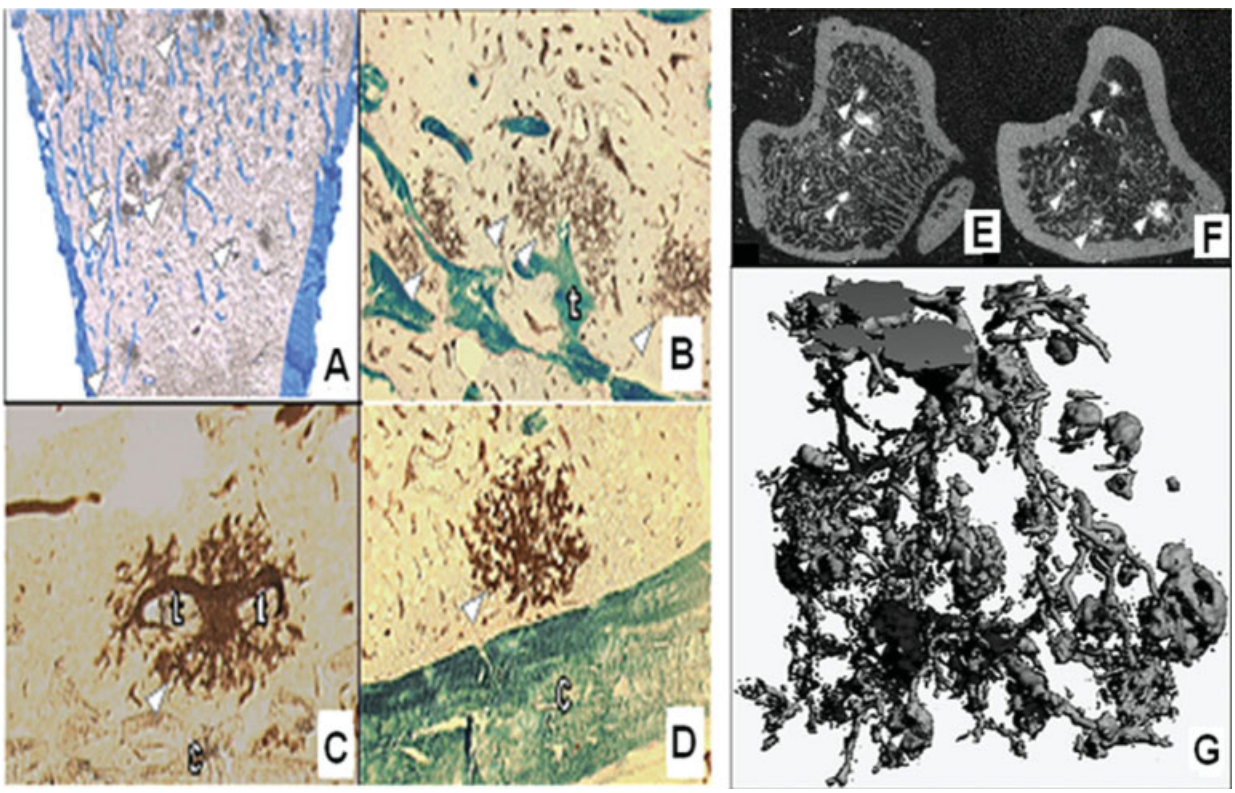

Fig. 8. Sinusoid capillary bundles imaging. (**A**–**D**) Histological sections of barium sulfate-infused tibia metaphysis. A: Original magnification: 40×. (B–D) Original magnification: 100×. (**E**–**G**) Images obtained with VivaCT40 (10 μm resolution), original magnification: 40×. Empty arrow heads: Sinusoid capillary bundles. (A) Upper metaphysis, (B) Secondary spongiosa (white t: trabecula), (C) Diaphysis (arrow: vessel supply of the sinusoid bundle), (D) In the vicinity of the bone cortical envelope (white c), (E, F) Transversal section images of non decalcified metaphysis at the junction between primary and secondary spongiosa (E) and between diaphysis and metaphysis (F). G: 3D image of sinusoid bundles spatial distribution in decalcified tibia metaphysis after removal of small vessels by size thresholding.

(Burrows et al., 2001) and limb angiogenesis in mice (Zhang et al., 2005). However, this preparation is not visible in histological sections and our main aim here was to compare quantitative data obtained with histomorphometry and μCT to validate μCT measurements. Furthermore, barium sulfate has been the contrasting agent used in Brookes and Revel's reference work for imaging bone vessels with microradiography (Brookes and Revell, 1998). Moreover, Micropaque® met the best requirements for correct opacification: its particles are spherical, homogeneous and micrometer sized while large enough to prevent diffusion through the vascular wall. Indeed, we did not observe any Barium sulfate grains in the bone marrow in the histological sections. Furthermore, barium solution behaves as a non-Newtonian liquid (Li et al., 1992) whose viscosity can decrease in vessels below 0.2–0.3 mm in diameter, providing that the flow shear rate is high enough. Most of all, barium sulfate (Micropaque®) was easily visualized and quantifiable in unstained histological sections. It exhibited excellent penetration and contrast effect in capillaries for both histological and 3D μCT analysis.

We previously described a bone vessel quantification technique using histological sections of India ink infused bones, based on manual counting with a 100-point grid and which has 10% reproducibility (Barou et al., 2002). In the present work, we show here a semiautomatic image analysis using the IMAGEJ 1.32J software, which is quicker and yields better CV.

Bone microvasculature was evaluated using micro-CT on two resolutions: 5 and 10 μm. In non decalcified bones, the substantial overlap between the linear attenuation coefficient (μ) of small vessels and bone trabeculae (vascular μ: 1.585 ∼ 8.00, bone matrix μ: 1.0 ∼ 3.0) forbade visualization of smaller vessels in the marrow and the cortices. In contrast, decalcification revealed a fully opacified vessel network that could be quantified using the software used for bone microarchitecture. Expectedly, vessel volumes and numbers were higher at the 5 μm resolution, probably due to the fact that smaller vessels were now included. Moreover, 3D μCT also show the significant reduction of bone vessel numbers in the tail suspension model. The higher resolution provided the more accurate parameters. This emphasized the potential use of this technique for quantitative assessment of the bone vascular network. Interestingly, the values obtained for vessel volumes were of similar order between the two techniques with little difference in range, (2.5%–6.5% and 3.0%–10.0% for histology and μCT, respectively).

In addition, this study provided greater 2D and 3D structural information of sinusoid clusters. Sinusoidal clusters are functional units playing a major role in the stem cell niche and may be the site where hematopoietic and osteogenic tissues interact (Yin and Li, 2006). Being able to follow the changes in these highly anastomosed vessel formations may permit further studies in their role in various stress conditions such as bone marrow transplantation recovery or hematopoiesis in ischemia.

In conclusion, we have demonstrated that barium sulfate was an adequate contrast agent for imaging and quantifying long bone vascularization in the rat. Moreover, we demonstrated that μCT, which provides high quality images of the bone microvascular network, is an accurate tool for assessing the changes in the complex anatomical structure of sinusoid clusters. This technique should facilitate further investigations to advance our understanding on the relationships between the bone and the vascular system.

ACKNOWLEDGMENTS

The authors thank Dr. Alain Guignandon for his generous help on IMAGE J.

LITERATURE CITED

Barou O, Mekraldi S, Vico L, Boivin G, Alexandre C, Lafage-Proust MH. 2002. Relationships between trabecular bone remodeling and bone vascularization: a quantitative study. Bone 30:604–612.

Bolland BJ, Kanczler JM, Dunlop DG, Oreffo RO. 2008. Development of in vivo muCT evaluation of neovascularisation in tissue engineered bone constructs. Bone 43:195–202.

Brookes M. 1960. Sequelae of experimental partial ischaemia in long bones of the rabbit. J Anat 94:552–561.

Brookes M, Revell W. 1998. Blood supply of bone: scientific aspects. 2nd ed. London: Springer-Verlag.

Burrows AM, O'Loughlin VD, Mooney MP, Smith TD, Losken HW, Siegel MI. 2001. Endocranial vascular patterns in a familial rabbit model of coronal suture synostosis. Cleft Palate Craniofac J 38:615–621.

Chappard D, Palle S, Alexandre C, Vico L, Riffat G. 1987. Bone embedding in pure methyl methacrylate at low temperature preserves enzyme activities. Acta Histochem 81:183–190.

Colleran PN, Wilkerson MK, Bloomfield SA, Suva LJ, Turner RT, Delp MD. 2000. Alterations in skeletal perfusion with simulated microgravity: a possible mechanism for bone remodeling. J Appl Physiol 89:1046–1054.

de Magalhaes RP, Ferraz AR, Brandao LG, Magalhaes MG. 1998. Osteogaleal pedicle flap of the occipital region for head and neck reconstruction–anatomic study. J Otolaryngol 27:195–199.

Duvall CL, Taylor WR, Weiss D, Guldberg RE. 2004. Quantitative microcomputed tomography analysis of collateral vessel development after ischemic injury. Am J Physiol Heart Circ Physiol 287:H302–310.

Elliott JC, Anderson P, Davis GR, Wong FSL, Dover SD. 1994. Computed topography. Part 2: the practical use of a single source and detector. J Microsc 126:11–19.

Fortepiani LA, Ruiz MC, Passardi F, Bentley MD, Garcia-Estan J, Ritman EL, Romero JC. 2003. Effect of losartan on renal microvasculature during chronic inhibition of nitric oxide visualized by micro-CT. Am J Physiol Renal Physiol 285:F852–860.

Harousseau JL, Shaughnessy J Jr., Richardson P. 2004. Multiple myeloma hematology. Am Soc Hematol Educ Program 237–256.

Kan Z, Kobayashi S, Phongkitkarun S, Charnsangavej C. 2005. Functional CT quantification of tumor perfusion after transhepatic arterial embolization in a rat model. Radiology 237:144–150.

Li M, Brasseur JG, Kern MK, Dodds WJ. 1992. Viscosity measurements of barium sulfate mixtures for use in motility studies of the pharynx and esophagus. Dysphagia 7:17–30.

Lorensen WE, Cline HE. 1987. Marching cubes: a high resolution 3D surface construction algorithm. ACM SIGGRAPH Comput Graph 21:163–169.

Lundberg LG, Lerner R, Sundelin P, Rogers R, Folkman J, Palmblad J. 2000. Bone marrow in polycythemia vera, chronic myelocytic leukemia, and myelofibrosis has an increased vascularity. Am J Pathol 157:15–19.

Mark H, Penington A, Nannmark U, Morrison W, Messina A. 2004. Microvascular invasion during endochondral ossification in experimental fractures in rats. Bone 35:535–542.

Momose A, Takeda T, Itai Y, Hirano K. 1996. Phase-contrast X-ray computed tomography for observing biological soft tissues. Nat Med 2:473–475.

Morey ER, Sabelman EE, Turner RT, Baylink DJ. 1979. A new rat model simulating some aspects of space flight. Physiologist 22:S23–24.

Parfitt AM, Drezner MK, Glorieux FH, Kanis JA, Malluche H, Meunier PJ, Ott SM, Recker RR. 1987. Bone histomorphometry: standardization of nomenclature, symbols, and units. Report of the ASBMR Histomorphometry Nomenclature Committee. J Bone Miner Res 2:595–610.

Parfitt AM, Mathews CH, Villanueva AR, Kleerekoper M, Frame B, Rao DS. 1983. Relationships between surface, volume, and thickness of iliac trabecular bone in aging and in osteoporosis. Implications for the microanatomic and cellular mechanisms of bone loss. J Clin Invest 72:1396–1409.

Plouraboue F, Cloetens P, Fonta C, Steyer A, Lauwers F, Marc-Vergnes JP. 2004. X-ray high-resolution vascular network imaging. J Microsc 215:139–148.

Salome M, Peyrin F, Cloetens P, Odet C, Laval-Jeantet AM, Baruchel J, Spanne P. 1999. A synchrotron radiation microtomography system for the analysis of trabecular bone samples. Med Phys 26:2194–2204.

Sasov A, Van Dyck D. 1998. Desktop X-ray microscopy and microtomography. J Microsc 191:151–158.

Schatteman GC, Awad O. 2004. Hemangioblasts, angioblasts, and adult endothelial cell progenitors. Anat Rec A Discov Mol Cell Evol Biol 276:13–21.

Toyota E, Fujimoto K, Ogasawara Y, Kajita T, Shigeto F, Matsumoto T, Goto M, Kajiya F. 2002. Dynamic changes in three-dimensional architecture and vascular volume of transmural coronary microvasculature between diastolic- and systolic-arrested rat hearts. Circulation 105:621–626.

Yin JJ, Pollock CB, Kelly K. 2005. Mechanisms of cancer metastasis to the bone. Cell Res 15:57–62.

Yin T, Li L. 2006. The stem cell niches in bone. J Clin Invest 116:1195–1201.

Zhang X, Xie C, Lin AS, Ito H, Awad H, Lieberman JR, Rubery PT, Schwarz EM, O'Keefe RJ, Guldberg RE. 2005. Periosteal progenitor cell fate in segmental cortical bone graft transplantations: implications for functional tissue engineering. J Bone Miner Res 20:2124–2137.